Applied Physics Letters

# Spin-controlled massive channels of hybrid-order Poincaré sphere beams

Cite as: Appl. Phys. Lett. **117**, 081101 (2020); https://doi.org/10.1063/5.0020398
Submitted: 30 June 2020 . Accepted: 13 August 2020 . Published Online: 25 August 2020

Yi-Heng Zhang, Peng Chen, Shi-Jun Ge, Ting Wei, Jie Tang, Wei Hu, and Yan-Qing Lu









AIP Publishing

# Spin-controlled massive channels of hybrid-order Poincaré sphere beams

Cite as: Appl. Phys. Lett. **117**, 081101 (2020); doi: 10.1063/5.0020398
Submitted: 30 June 2020 · Accepted: 13 August 2020 ·
Published Online: 25 August 2020

View Online Export Citation CrossMark

Yi-Heng Zhang,[1] Peng Chen,[1,a)] Shi-Jun Ge,[1] Ting Wei,[1] Jie Tang,[1,2] Wei Hu,[1] and Yan-Qing Lu[1,a)]

## AFFILIATIONS

[1]National Laboratory of Solid State Microstructures, Key Laboratory of Intelligent Optical Sensing and Manipulation, College of Engineering and Applied Sciences, and Collaborative Innovation Center of Advanced Microstructures, Nanjing University, Nanjing 210093, China

[2]Department of Physics, Nantong University, Nantong 226019, China

[a)]Authors to whom correspondence should be addressed: chenpeng@nju.edu.cn and yqlu@nju.edu.cn

## ABSTRACT

Featuring a nontrivial coupling between the orbital angular momentum of light and spatially inhomogeneous polarization, hybrid-order Poincaré sphere (HyOPS) beams have recently triggered numerous curiosities, especially in classical and quantum informatics. Despite much effort devoted to creating single HyOPS beam, it is still a formidable challenge to simultaneously harness multichannel and diverse HyOPS beams in a simple and efficient manner. Here, we propose a digitalized geometric phase optical element via photo-induced liquid crystal microstructures and demonstrate flexible and spin-controlled massive channels of HyOPS beams. By tuning the incident polarization, any state on up to 24 diverse HyOPSs is simultaneously mapped from common Poincaré sphere in high efficiency and good energy uniformity. All experimental results match well with the theoretical predictions of such a planar multifunctional device. This adds an extra spatial degree of freedom to advanced light tailoring and may facilitate parallel optical trapping, high-capacity communication, and high-dimensional quantum entanglement.



Vector vortex beam (VVB), characterized by helicoidal transverse polarization and a spiral phase structure, has attracted ever-increasing interest. Compared with the optical vortex[1] of homogeneous polarization and vector beam[2] of flat wave-front, VVB carries both spin and orbital angular momentum (SAM/OAM) of light simultaneously, offering a much higher degree of freedom in light–matter interaction,[3,4] high-resolution imaging,[5] and optical communication.[6] In particular, the inherently hyper-entanglement between its polarization and spatial degree of freedom makes VVB a versatile protocol for quantum information processing.[7,8] Referring to the well-known Poincaré sphere, the theoretical framework of hybrid-order Poincaré sphere (HyOPS)[9] has recently been proposed to describe complex polarization states of VVBs. For instance, a HyOPS with the topological charge $m = +3$ and $l = +1$ is illustrated in Fig. 1(a). North/south pole represents the right/left circularly polarized optical vortex carrying a SAM of $-\hbar/+\hbar$ and an OAM of $m\hbar/l\hbar$.[10] Any other point on the HyOPS is the linear superposition of two such eigenstates. The equator denotes VVBs with both spatially variant polarization and phase, resulting in the dark central and partly separated lobes after passing through an analyzer. In the case of $m = -l$, the HyOPS reduces to the so-called higher-order Poincaré sphere,[11,12] whose equator indicates cylindrical vector beams with only one central polarization singularity and transforms to disconnected lobes accordingly.

On-demand engineering of HyOPS beams lies in the heart of their fundamental research and cutting-edge applications. Generally, generation strategies can be divided into two major types. One is independently manipulating and then combining two eigenstates of the desired HyOPS. Spatial light modulators (SLMs) are usually employed with the collaboration of an interferometer or prism.[13–15] The other is based on the geometric phase originating from the spin–orbit interaction of light.[16] Inhomogeneous anisotropic media are indispensable, among which metasurface-based spin-controlled light manipulation has been extensively studied.[17–21] Despite the impressive progress aimed at single HyOPS using cascaded liquid crystal (LC) devices[22,23] and modified metasurfaces,[24–26] only limited works[27–29] involve the simultaneous acquisition of multichannel HyOPS beams while also facing challenging issues in system complexity, optical efficiency, and channel scale. Driven by promising opportunities in multiple optical tweezers,[30] parallel laser manufacturing,[31] and high-dimensional

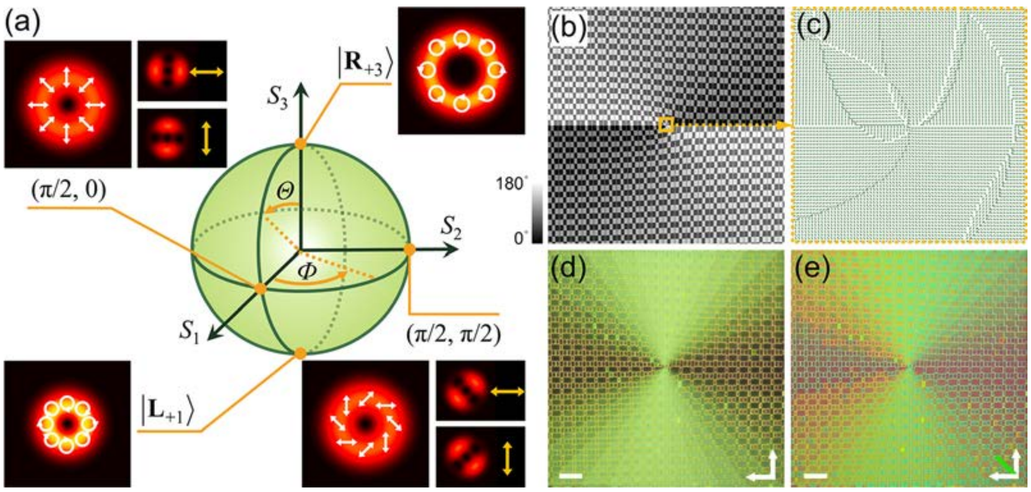


FIG. 1. (a) Schematic illustration of a HyOPS with $m = +3$ and $l = +1$. $(\Theta, \Phi)$ is the spherical coordinate. For certain points, intensity profiles and polarization distributions (white arrows) are presented with transformed patterns after transmitting an analyzer (yellow arrows). (b) Theoretically designed optical axis distribution of a Dammann-vortex-$q$-plate (DVQP) with $N_x = 5$, $N_y = 2$, $m_x = +1$, $m_y = +2$, and $q = +0.5$. The color variation from black to white indicates the axis varying from 0° to 180°. (c) Enlarged details in the central region of (b) and green short sticks denote the local optical axis orientations. Polarized optical micrograph (d) without and (e) with a sensitive tint plate (i.e., the full-wave plate at $\lambda = 530$ nm). All scale bars are 100 $\mu$m.

classical/quantum informatics, a compact, effective, and flexible scheme to harness massive HyOPS channels is highly desirable.

In this work, a special LC geometric phase element is proposed by digitalizing the conventional spiral phase with the Dammann vortex grating (DVG), and massive channels of HyOPS beams are achieved directly. Via such a single planar device, a large beam lattice with each order corresponding to a different HyOPS is obtained in good quality and relatively uniform energy distribution. The merit of spin dependence enables the simultaneous mapping from common Poincaré sphere to multiple diverse HyOPSs. Moreover, to extend the channel scale, the designed structure is further optimized and a 24-channel HyOPS beam is demonstrated. This supplies a robust and convenient method for large-scale manipulation of VVBs and other structured light.

To enable the parallel beam manipulating, the concept of Dammann grating is usually introduced.[32,33] DVG is a binary-phase (0 and $\pi$) forked grating composed of a set of specific phase transition points. Here, we imprint the two-dimensional DVG into the $q$-plate[34] by encoding the binary phase of DVG to traditional spiral geometric phase. Such a process can be an analogy with the computer binary system, so we call it "digitalizing," which denotes an integration of binary and space-variant geometric phases.[12,35] Accordingly, a fancy digitalized geometric phase optical element is obtained, named as Dammann-vortex-$q$-plate (DVQP). The transmission function of a one-dimensional DVG with the phase profile $\varphi_{x\text{-DVG}}(x)$ is expressed as[33]

$$T(x) = \exp\left(\mathrm{i}\varphi_{x-\mathrm{DVG}}(x)\right) = \sum_{p=-\infty}^{+\infty} C_p \exp\left[\mathrm{i}p \times \left(m_x\phi + \frac{2\pi x}{\Lambda_x}\right)\right], \tag{1}$$

where $m_x$ is the topological charge of DVG, $\phi = \arctan(y/x)$ is the azimuth angle, and $\Lambda_x$ is the period. $|C_p|^2$ is the power ratio of the $p$th diffraction order to the total. Through optimizing the number and values of phase transition points in the DVG, the incident light can be diffracted into $N_x$ desired OAM modes with equal-energy distribution. As an example of $N_x = 5$, normalized phase transition points can be selected as $x_0 = 0$, $x_1 = 0.03863$, $x_2 = 0.39084$, $x_3 = 0.65552$, and $x_4 = 1$, respectively.[32] By integrating two orthogonal one-dimensional DVG, a two-dimensional DVG is formed and further encoded into the $q$-plate. Accordingly, the optical axis orientation of such a DVQP can be formulated as

$$\alpha = q\phi + \frac{1}{2}\varphi_{x\text{-DVG}} + \frac{1}{2}\varphi_{y\text{-DVG}}, \tag{2}$$

where $q$ is the topological charge of the initial $q$-plate. For instance, Fig. 1(b) presents a DVQP with $N_x = 5$, $N_y = 2$, $m_x = +1$, $m_y = +2$, and $q = +0.5$, whose space-variant optical axes are exhibited by gray color. The central region is enlarged and vividly depicted by green short sticks in Fig. 1(c).

As a convenient theoretical tool, the Jones matrix calculation[36] is employed to derive the diffraction properties resulting from the spin–orbit interaction of light. Jones vectors of left and right circular polarization (LCP/RCP) are $|\mathbf{L}\rangle = [1 \quad \mathrm{i}]^{\mathrm{T}}/\sqrt{2}$ and $|\mathbf{R}\rangle = [1 \quad -\mathrm{i}]^{\mathrm{T}}/\sqrt{2}$, respectively. Thus, the incident light with arbitrary polarization state can be decomposed as

$$|\psi_{\mathrm{in}}\rangle = \cos\left(\frac{\Theta}{2}\right)\mathrm{e}^{-i\Phi/2}|\mathbf{L}\rangle + \sin\left(\frac{\Theta}{2}\right)\mathrm{e}^{+i\Phi/2}|\mathbf{R}\rangle, \tag{3}$$

where $(\Theta, \Phi)$ is the spherical coordinate on the conventional Poincaré sphere. Considering $\alpha$ in the half-wave condition, the Jones matrix of the DVQP can be described as

$$\mathbf{J} = \begin{bmatrix} \cos(2\alpha) & \sin(2\alpha) \\ \sin(2\alpha) & -\cos(2\alpha) \end{bmatrix}. \tag{4}$$

Therefore, the output light follows

$$
\begin{aligned}
|\psi_{\text{out}}\rangle &= \mathbf{J}|\psi_{\text{in}}\rangle \\
&= \cos\left(\frac{\Theta}{2}\right)e^{-i\Phi/2}|\mathbf{R}\rangle e^{+i2\alpha} + \sin\left(\frac{\Theta}{2}\right)e^{+i\Phi/2}|\mathbf{L}\rangle e^{-i2\alpha} \\
&= \left[\cos\left(\frac{\Theta}{2}\right)e^{-i\Phi/2}|\mathbf{R}\rangle e^{+i2q\phi} + \sin\left(\frac{\Theta}{2}\right)e^{+i\Phi/2}|\mathbf{L}\rangle e^{-i2q\phi}\right] \\
&\quad \times e^{i\varphi_{x-\text{DVG}}+i\varphi_{y-\text{DVG}}} \\
&= \sum_{p=-\infty}^{+\infty}\sum_{s=-\infty}^{+\infty} C_p C_s \exp\left(i\frac{2\pi px}{\Lambda_x} + i\frac{2\pi sy}{\Lambda_y}\right)|\psi_{p,s}\rangle,
\end{aligned} \tag{5}
$$

where

$$
\begin{aligned}
|\psi_{p,s}\rangle &= \cos\left(\frac{\Theta}{2}\right)e^{-i\Phi/2}|\mathbf{R}\rangle e^{+i(pm_x+sm_y+2q)\phi} \\
&\quad + \sin\left(\frac{\Theta}{2}\right)e^{+i\Phi/2}|\mathbf{L}\rangle e^{+i(pm_x+sm_y-2q)\phi} \\
&= \cos\left(\frac{\Theta}{2}\right)e^{-i\Phi/2}|\mathbf{R}_{pm_x+sm_y+2q}\rangle + \sin\left(\frac{\Theta}{2}\right)e^{+i\Phi/2}|\mathbf{L}_{pm_x+sm_y-2q}\rangle.
\end{aligned} \tag{6}
$$

The resultant geometric phase $\pm 2\alpha$ from the DVQP contributes to an $N_y \times N_x$ beam channel determined by the Dammann phase transition points, where the diffraction order ($p$th, $s$th) corresponds to a distinctive HyOPS with $m = pm_x + sm_y + 2q$ and $l = pm_x + sm_y - 2q$. Moreover, the spin mapping is verified from the point ($\Theta$, $\Phi$) on the Poincaré sphere to the same point on the HyOPS. Consequently, by precisely designing structure parameters ($N_x$, $N_y$, $m_x$, $m_y$, and $q$) of the DVQP, the incident light can be equally diffracted into massive channels of diverse HyOPS beams, and the state of each channel can be flexibly controlled via the incident SAM.

As a natural birefringent material with controllable and stimuli-responsive self-assembly behavior, LCs have been witnessed with enormous advances in geometric phase planar optics.[37] Here, the polarization-sensitive azo-dye SD1[38]-based dynamic photo-patterning technology[39] was adopted to imprint the designed optical axis orientation into nematic LCs. After exposing an empty 6-$\mu$m-thick cell with the multi-step partly overlapping process[12,40] and filling LC E7, a DVQP can be fabricated with a period of 48 $\mu$m. Figure 1(d) shows the optical micrograph recorded under crossed polarizers. The continuous changing brightness is induced by space-variant LC directors corresponding to Figs. 1(b) and 1(c), while the forked net-like disclinations are attributed to the 90° director shift astride domain boundaries. Taking a full-wave plate ($\lambda = 530$ nm) inserted at 45° to the crossed polarizers as a sensitive tint plate, an enhanced anisotropic texture is obtained in Fig. 1(e). The experimental director distribution is vividly revealed, verifying a faithful transformation from the theoretical design to the LC layer.

The generation and analysis of multichannel HyOPS beams are accomplished by the optical setup schematically exhibited in Fig. 2(a). The incident monochromatic laser with $\lambda = 632.8$ nm and a beam diameter of 1 mm is adjusted to the desired polarization state via a half-wave plate and a quarter-wave plate. The diffraction pattern is recorded on the screen at a distance of 75 cm and captured by a camera. During the whole experiment, a voltage of 2.4 V is applied on the LC cell to satisfy the half-wave condition for 632.8 nm. When $|\psi_{\text{in}}\rangle = |\mathbf{L}\rangle$, a $2 \times 5$ channel of RCP donut-like beams is generated, as shown in Fig. 2(c), which matches well with the theoretical simulation in Fig. 2(b). The (+1st, −1st) order exhibits a bright central spot, indicating the Gaussian mode. Based on the astigmatic transformation,[39] a cylindrical lens ($f = 100$ mm) is placed between the DVQP and a charge-coupled device (CCD) to measure the topological charge distribution. Through the number and tilt direction of dark stripes, the converted pattern in Fig. 2(d) shows that the topological charge ranges from $m = -3$ to $m = +5$ and ($p$th, $s$th) OAM order follows $m = p + 2s + 1$, consistent with Eq. (6). These channels correspond to eigenstates on the north poles of diverse HyOPSs. While for $|\psi_{\text{in}}\rangle = |\mathbf{R}\rangle$, the output turns to the respective south poles as simulated in Fig. 2(e) and recorded in Fig. 2(f), which looks centrosymmetric to that of $|\psi_{\text{in}}\rangle = |\mathbf{L}\rangle$. The OAM detection result shown in Fig. 2(g) denotes a range from $l = -5$ to $l = +3$, formulated as $l = p + 2s - 1$. The diffraction efficiency of each desired HyOPS order is measured as an average value of 5.77% with a fluctuation within ± 0.64%. The total efficiency approaches 58%, consistent with the theoretical value 62.72%.[32] These indicate that a high efficiency together with a good energy uniformity is achieved, thanks to the LC mediated geometric phase.[37] Accordingly, by alternating the incident spin, massive channels of OAM eigenstates on different HyOPSs can be dynamically switched.

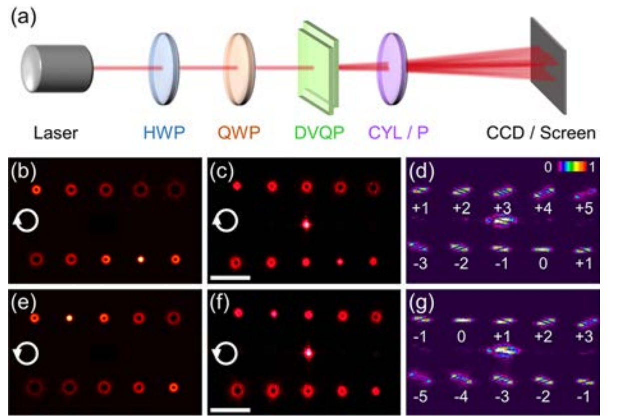


**FIG. 2.** (a) Optical setup to generate and analyze multichannel HyOPS beams. HWP, half-wave plate; QWP, quarter-wave plate; CYL, cylindrical lens; P, polarizer. Theoretical and experimental diffraction patterns at 632.8 nm with (b) and (c) LCP and (e) and (f) RCP incident, respectively. (d) and (g) Corresponding converted patterns captured in the focal plane of the cylindrical lens. All scale bars are 1 cm.

In addition to polar eigenstates, VVBs on equators of multiple HyOPSs are also created. As a representative case, the horizontal linear polarization is incident to generate the equatorial point ($\pi/2$, 0) on the HyOPS, where two orthogonal eigenstates are equally weighted. To reveal the polarization distributions of VVBs, another polarizer is used and the corresponding results are shown in Fig. 3. Three typical orders are selected as examples for clarification and illustrated on the respective HyOPS. As a superposition of $|\mathbf{R}_{+3}\rangle$ and $|\mathbf{L}_{+1}\rangle$, order I corresponds to the HyOPS shown in Fig. 1(a). Order II, characterized by a bright center, is composed of a Gaussian mode and an OAM mode with $l = -2$. Order III is a standard cylindrical vector beam, located on the higher-order Poincaré sphere with $m = -l = 1$. The transmitted intensity profile of order III is observed as two disconnected lobes parallel to the analyzer orientation. In all, we obtain 10 different HyOPS channels in relatively equal energy distribution.

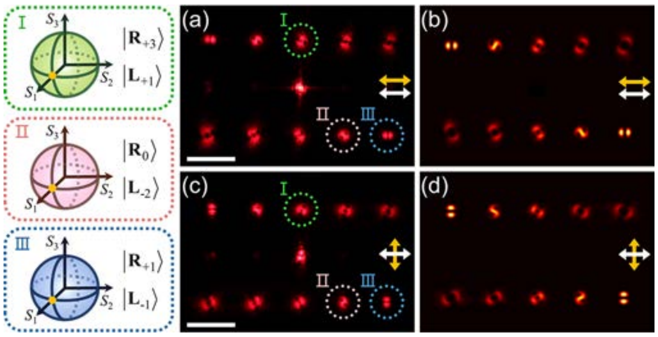


FIG. 3. Experimental and theoretical diffraction patterns with the horizontally polarized incident light after transmission through (a) and (b) horizontal and (c) and (d) vertical analyzers, respectively. White arrows represent the incident polarization, while yellow arrows represent the rotating analyzer. (0th, +1st), (+1st, −1st), and (+2nd, −1st) orders are labeled as I, II, and III and located on the corresponding HyOPS, respectively. All scale bars are 1 cm.

Although all transmitted orders have the similar shape featuring two main lobes, the intensity minima orient at different azimuthal directions, which could be attributed to the Gouy phase of the Laguerre–Gaussian mode.[27,41] For horizontal polarizer and analyzer in Fig. 3(a), the intensity profile will find its minima at azimuth angles $\phi_k = \frac{(2k+1)\pi}{m-l} + \frac{(|m|-|l|)\zeta}{m-l}$, where $k$ is an integer from 1 to $|m-l|$ and $\zeta = \arctan(z\lambda/\pi w_0^2)$.[27,41] It is noteworthy that such a dependence on the Gouy phase during the propagation provides an additional degree of freedom to manipulating VVBs. All experimental results are consistent with theoretical simulations. Besides the high-quality generation of equatorial VVBs, any other states on diverse HyOPSs can be flexibly produced by controlling the incident polarization.

To further expand the channel scale of diverse HyOPS beams, Dammann structure parameters can be properly optimized. A DVQP with $N_x = 5$, $N_y = 5$, $m_x = +1$, $m_y = +5$, and $q = +1$ is demonstrated, whose optical axis distribution and the micrograph are shown in Figs. 4(a) and 4(b), respectively. Thanks to the electrical tunability of LC materials, the same device can work at different wavelengths. For $\lambda = 532$ nm, the applied voltage increases to 2.7 V to keep the half-wave condition, achieving the maximum diffraction efficiency and an equivalent performance. When $|\psi_{in}\rangle = |\mathbf{L}\rangle$, $5 \times 5$ channels of RCP OAM modes ranging from $m = -10$ to $m = +14$ are observed in Fig. 4(c). While for the horizontally polarized incident combined with a crossed analyzer, VVBs on 24 different HyOPSs are generated simultaneously, as exhibited in Fig. 4(d). Such large topological charges and channel number verify its great capability of parallel beam tailoring. Diffraction efficiency of each main order lies within the range of 2.27% ± 0.92%. High OAM order exhibits a significantly increased efficiency compared with the common forked grating, despite a little poorer energy uniformity. This is attributed to the fabrication deviation from theoretical fine structures, as verified by partly missing narrow lines and few greenish rectangles in their micrographs. Performances of DVQP can be further improved via photo-patterning systems with a much higher resolution.[37]

In summary, spin-controlled massive channels of HyOPS beams are flexibly realized via an LC-mediated geometric phase element. By digitalizing the spiral phase with the unique binary structure of the DVG, up to 24 channels of diverse VVBs are generated directly in high efficiency and relatively uniform energy distribution. The state of each channel can be arbitrarily selected by controlling the incident SAM. Additionally, merits of planar configuration, compact volume, and electro-optical tunability make it practical and effective. Actually, the arbitrary control of OAM order in each channel could be reasonably expected by referring the design principle of relevant metasurfaces.[27,42] Electrical switching of multi-channel HyOPS is also achievable by further integrating a tunable LC wave-plate.[23,43] This work advances the on-demand engineering of VVBs and provides more potentials in various fields, including optical manipulation, fabrication, and communication.

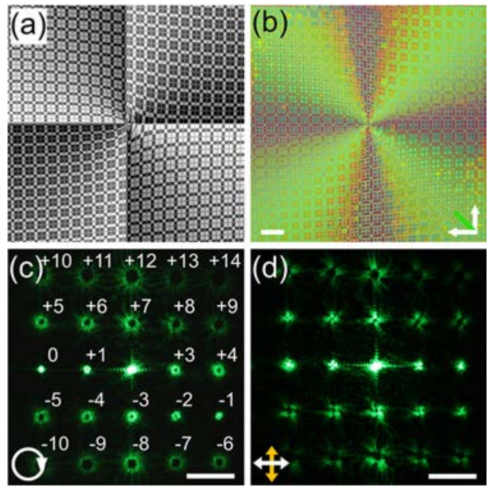


FIG. 4. (a) Theoretically designed optical axis distribution and (b) polarized optical micrograph with a sensitive tint plate of a DVQP with $N_x = 5$, $N_y = 5$, $m_x = +1$, $m_y = +5$, and $q = +1$. The color variation from black to white indicates the axis varying from 0° to 180°. Scale bar in (b) is 100 $\mu$m. Diffraction patterns at 532 nm with the incident of (c) LCP and (d) horizontal polarization after transmission through a vertical analyzer. Scale bars in (c) and (d) are 1 cm.

This work was supported by the National Key Research and Development Program of China (No. 2017YFA0303700), the National Natural Science Foundation of China (NSFC) (No. 61922038), the Natural Science Foundation of Jiangsu Province (Nos. BK20180004 and SBK2020044418), and the Fundamental Research Funds for the Central Universities (No. 021314380001).

## DATA AVAILABILITY

The data that support the findings of this study are available from the corresponding author upon reasonable request.

## REFERENCES

[1]Y. J. Shen, X. J. Wang, Z. W. Xie, C. J. Min, X. Fu, Q. Liu, M. L. Gong, and X. C. Yuan, Light Sci. Appl. 8, 90 (2019).
[2]Q. Zhan, Adv. Opt. Photonics 1, 1–57 (2009).
[3]D. L. Gao, W. Q. Ding, M. Nieto-Vesperinas, X. M. Ding, M. Rahman, T. H. Zhang, C. Lim, and C. W. Qiu, Light Sci. Appl. 6, e17039 (2017).
[4]E. Allahyari, J. JJ Nivas, F. Cardano, R. Bruzzese, R. Fittipaldi, L. Marrucci, D. Paparo, A. Rubano, A. Vecchione, and S. Amoruso, Appl. Phys. Lett. 112, 211103 (2018).
[5]L. Yan, P. Gregg, E. Karimi, A. Rubano, L. Marrucci, R. Boyd, and S. Ramachandran, Optica 2, 900–903 (2015).

[6]A. E. Willner, H. Huang, Y. Yan, Y. Ren, N. Ahmed, G. Xie, C. Bao, L. Li, Y. Cao, Z. Zhao, J. Wang, M. P. J. Lavery, M. Tur, S. Ramachandran, A. F. Molisch, N. Ashrafi, and S. Ashrafi, Adv. Opt. Photonics **7**, 66–106 (2015).
[7]M. Malik, M. Erhard, M. Huber, M. Krenn, R. Fickler, and A. Zeilinger, Nat. Photonics **10**, 248–252 (2016).
[8]F. Flamini, N. Spagnolo, and F. Sciarrino, Rep. Prog. Phys. **82**, 016001 (2019).
[9]X. N. Yi, Y. C. Liu, X. H. Ling, X. X. Zhou, Y. G. Ke, H. L. Luo, S. C. Wen, and D. Y. Fan, Phys. Rev. A **91**, 023801 (2015).
[10]L. Allen, M. W. Beijersbergen, R. J. Spreeuw, and J. P. Woerdman, Phys. Rev. A **45**, 8185–8189 (1992).
[11]G. Milione, H. I. Sztul, D. A. Nolan, and R. R. Alfano, Phys. Rev. Lett. **107**, 053601 (2011).
[12]P. Chen, S. J. Ge, W. Duan, B. Y. Wei, G. X. Cui, W. Hu, and Y. Q. Lu, ACS Photonics **4**, 1333–1338 (2017).
[13]X. H. Ling, X. N. Yi, Z. P. Dai, Y. W. Wang, and L. Z. Chen, J. Opt. Soc. Am. B **33**, 2172–2176 (2016).
[14]S. Y. Fu, Y. W. Zhai, T. L. Wang, C. Yin, and C. Q. Gao, Appl. Phys. Lett. **111**, 211101 (2017).
[15]C. L. Chang, L. Li, Y. Gao, S. P. Nie, Z. C. Ren, J. P. Ding, and H. T. Wang, Appl. Phys. Lett. **114**, 041101 (2019).
[16]E. Cohen, H. Larocque, F. Bouchard, F. Nejadsattari, Y. Gefen, and E. Karimi, Nat. Rev. Phys. **1**, 437–449 (2019).
[17]H. X. Xu, G. W. Hu, L. Han, M. H. Jiang, Y. J. Huang, Y. Li, X. M. Yang, X. H. Ling, L. Z. Chen, J. L. Zhao, and C. W. Qiu, Adv. Opt. Mater. **7**, 1801479 (2018).
[18]J. X. Zhou, H. L. Qian, G. W. Hu, H. L. Luo, S. C. Wen, and Z. W. Liu, ACS Nano **12**, 82–88 (2018).
[19]G. W. Hu, X. M. Hong, K. Wang, J. Wu, H. X. Xu, W. C. Zhao, W. W. Liu, S. Zhang, F. Garcia-Vidal, B. Wang, P. X. Lu, and C. W. Qiu, Nat. Photonics **13**, 467–472 (2019).
[20]H. X. Xu, G. W. Hu, Y. Li, L. Han, J. L. Zhao, Y. M. Sun, F. Yuan, G. M. Wang, Z. H. Jiang, X. H. Ling, T. J. Cui, and C. W. Qiu, Light Sci. Appl. **8**, 3 (2019).
[21]H. X. Xu, G. W. Hu, M. H. Jiang, S. W. Tang, Y. Z. Wang, C. H. Wang, Y. J. Huang, X. H. Ling, H. W. Liu, and J. F. Zhou, Adv. Mater. Technol. **5**, 1900710 (2020).
[22]M. J. Tang, P. Chen, W. L. Zhang, A. M. W. Tam, V. G. Chigrinov, W. Hu, and Y. Q. Lu, Opt. Express **24**, 25510–25514 (2016).
[23]S. Z. Lou, Y. Q. Zhou, Y. D. Yuan, T. G. Lin, F. Fan, X. Q. Wang, H. H. Huang, and S. C. Wen, Opt. Express **27**, 8596–8604 (2019).
[24]F. Y. Yue, D. D. Wen, J. T. Xin, B. D. Gerardot, J. S. Li, and X. Z. Chen, ACS Photonics **3**, 1558–1563 (2016).
[25]Z. X. Liu, Y. Y. Liu, Y. G. Ke, Y. C. Liu, W. Shu, H. L. Luo, and S. C. Wen, Photonics Res. **5**, 15–21 (2017).
[26]Y. J. Bao, J. C. Ni, and C. W. Qiu, Adv. Mater. **32**, 1905659 (2020).
[27]F. Y. Yue, D. D. Wen, C. M. Zhang, B. D. Gerardot, W. Wang, S. Zhang, and X. Z. Chen, Adv. Mater. **29**, 1603838 (2017).
[28]S. Y. Fu, T. L. Wang, Z. Y. Zhang, Y. W. Zhai, and C. Q. Gao, Appl. Phys. Lett. **110**, 191102 (2017).
[29]Y. Chen, K. Y. Xia, W. G. Shen, J. Gao, Z. Q. Yan, Z. Q. Jiao, J. P. Dou, H. Tang, Y. Q. Lu, and X. M. Jin, Phys. Rev. Lett. **124**, 153601 (2020).
[30]L. Anderegg, L. W. Cheuk, Y. Bao, S. Burchesky, W. Ketterle, K. K. Ni, and J. M. Doyle, Science **365**, 1156–1158 (2019).
[31]Y. Li and M. H. Hong, Laser Photonics Rev. **14**, 1900062 (2020).
[32]C. H. Zhou and L. R. Liu, Appl. Opt. **34**, 5961–5969 (1995).
[33]T. Lei, M. Zhang, Y. Li, P. Jia, G. N. Liu, X. G. Xu, Z. H. Li, C. J. Min, J. Lin, C. Y. Yu, H. B. Niu, and X. C. Yuan, Light Sci. Appl. **4**, e257 (2015).
[34]L. Marrucci, C. Manzo, and D. Paparo, Phys. Rev. Lett. **96**, 163905 (2006).
[35]R. Xu, P. Chen, J. Tang, W. Duan, S. J. Ge, L. L. Ma, R. X. Wu, W. Hu, and Y. Q. Lu, Phys. Rev. Appl. **10**, 034061 (2018).
[36]P. Yeh and C. Gu, *Optics of Liquid Crystal Displays* (John Wiley & Sons, 1999).
[37]P. Chen, B. Y. Wei, W. Hu, and Y. Q. Lu, Adv. Mater. **32**, 1903665 (2019).
[38]V. Chigrinov, S. Pikin, A. Verevochnikov, V. Kozenkov, M. Khazimullin, J. Ho, D. D. Huang, and H. S. Kwok, Phys. Rev. E **69**, 061713 (2004).
[39]P. Chen, L. L. Ma, W. Hu, Z. X. Shen, H. K. Bisoyi, S. B. Wu, S. J. Ge, Q. Li, and Y. Q. Lu, Nat. Commun. **10**, 2518 (2019).
[40]P. Chen, B. Y. Wei, W. Ji, S. J. Ge, W. Hu, F. Xu, V. G. Chigrinov, and Y. Q. Lu, Photonics Res. **3**, 133–139 (2015).
[41]S. M. Baumann, D. M. Kalb, L. H. MacMillan, and E. J. Galvez, Opt. Express **17**, 9818–9827 (2009).
[42]Z. H. Jiang, L. Kang, T. Yue, H. X. Xu, Y. Yang, Z. Jin, C. Yu, W. Hong, D. H. Werner, and C. W. Qiu, Adv. Mater. **32**, 1903983 (2020).
[43]Y. Liu, P. Chen, R. Yuan, C. Q. Ma, Q. Guo, W. Duan, V. G. Chigrinov, W. Hu, and Y. Q. Lu, Opt. Express **27**, 36903–36910 (2019).